ELSEVIER

Materials Science and Engineering A 490 (2008) 117–125

MATERIALS SCIENCE & ENGINEERING A

www.elsevier.com/locate/msea

Tensile deformation and fracture behaviors of high purity polycrystalline zinc

J.H. Liu*, C.X. Huang, S.D. Wu, Z.F. Zhang

Shenyang National Laboratory for Materials Science, Institute of Metal Research, Chinese Academy of Sciences, Shenyang 110016, People's Republic of China

Received 21 October 2007; received in revised form 26 December 2007; accepted 2 January 2008

Abstract

The damage and fracture behaviors of high purity polycrystalline zinc with two grain sizes during tension were investigated experimentally at different strain rates. It was found that specimens with coarse grains (~1 mm) showed serrated flow behavior and failed in intermittent brittle cleavage fracture, while specimens with fine grains (~70 μm) showed no cleavage crack initiation before necking even at high strain rate. It was observed that the fracture process of the fine-grained specimen was highly related to strain rates. With the strain rate increasing, the damage mechanism transformed from formation of tearing cracks along interfaces (including grain boundaries, twin boundaries and kink band boundaries) and cavity coalescence into abrupt quasi-cleavage fracture. Based on the observation, the inter-crystalline fracture of zinc was investigated, and the damage and fracture behaviors of polycrystalline zinc during tension at room temperature were discussed in general.

Keywords: Zinc; Tension; Fracture; Cleavage; Cavity

1. Introduction

Zinc is a typical metal with hexagonal close-packed (HCP) lattice structure. Its *c/a* ratio (1.856) is higher than those of other HCP metals except Cd, which makes its independent slip and twinning systems relatively few [1–5]. At the same time, its cleavage plane coincides with its primary slip plane, which makes it incline to form cleavage cracks and show brittle fracture behaviors [1,6,7]. On the other hand, the activation energy of zinc is fairly low (as listed in Table 1 [8]) and room temperature (298.15 K) has reached 0.43 of the melting point (692.65 K) of zinc, suggesting that the diffusion and transition of point defects as well as dislocations are relatively intense even at room temperature. Thus, the behaviors of grain boundaries, such as grain boundary sliding, may affect the deformation and fracture process. Consequently, the deformation and fracture of polycrystalline zinc at room temperature should be influenced both by its special crystal structure and normally considered high temperature deformation behaviors.

The fracture behaviors of mono- and bi-crystal zinc were widely investigated in the past [9–14]. It was generally considered that tension of mono-crystal zinc would induce formation of twinning intersection and bunched slip bands, which resulted in local intense stress concentration and led to subsequent cleavage crack initiation in mono-crystal. As for bi-crystal, stress concentration near grain boundaries during tension served as the primary cause for cleavage initiation. In particular, Schmitz et al. made a brief review of the past research on deformation and fracture of zinc and investigated the fracture process of bi-crystal zinc in detail. He considered that cleavage crack initiated in BAZ (boundary affected zone) which was created by non-basal slip in a region close to the boundary during deformation, and the resistance for the crack to penetrate into another grain was associated with grain boundary type [14]. Although the fracture behaviors of mono- and bi-crystal zinc were studied deeply, there had been few researches on the fracture of polycrystalline zinc. Recent study showed that coarse-grained polycrystalline zinc failed in intermittent cleavage during compression and fatigue and showed similar features as in bi-crystal [7,15]. However, it was well known that most zinc alloy systems showed super-plasticity at low temperature [16,17], which suggested that polycrystalline zinc could potentially show good

* Corresponding author. Tel.: +86 24 83978270; fax: +86 24 23971320.
E-mail address: jhliu@imr.ac.cn (J.H. Liu).

0921-5093/$ – see front matter © 2008 Elsevier B.V. All rights reserved.
doi:10.1016/j.msea.2008.01.004

Table 1
Activation energy of metals for lattice diffusion, boundary diffusion and power-law creep [6]

Element	$Q_{\text{lattice diffusion}}$ (kJ/mol)	$Q_{\text{boundary diffusion}}$ (kJ/mol)	$Q_{\text{power-law creep}}$ (kJ/mol)
Zn	91.7	60.5	152
Pb	109	66	–
Mg	135	92	230
Al	142	84	–
α-Ti	150	97	242

plasticity and fracture in a mode rather different from cleavage even at room temperature. Actually, inter-granular cracking was clearly observed in zinc coatings on hot-dip galvanized steel during tension test [18,19]. Thus, it was inadequate to conclude all the fracture behaviors of polycrystalline zinc from the knowledge on mono- and bi-crystals.

Through varying grain size and strain rate, the purpose of the present work is to make a general investigation of the deformation and fracture behaviors of polycrystalline zinc via detailed observation using SEM, during which the deformation of material in the vicinity of grain boundaries was specially considered.

2. Experimental details

99.999% high purity distilled cast zinc sticks were used as the raw material. Firstly, the zinc sticks were placed into a vacuum furnace with a graphite mold. After that, the vacuum furnace was degassed to 10^{-6} atm and then filled with argon to 1.5 atm. This procedure was repeated twice to eliminate oxygen. Subsequently, the material was melted in argon at 520 °C and kept for 4 h. Finally, 12 mm thick cast zinc plates were obtained. After that, the zinc plates were hot-rolled to 6 mm thick at 320 °C and were cooled to room temperature in air. Then tensile specimens were spark cut from the as-rolled zinc plates with gauge lengths of 20 mm and cross-sectional areas of 44 mm^2 (Fig. 1). Finally, one group of the specimens was annealed at 150 °C for 2 h, while the other group was annealed at 260 °C for 2 h to yield coarse grains.

In order to investigate the microstructures, the specimens annealed at 150 °C were treated with solution composed of 20 g CrO_3, 1.5 g Na_2SO_4 and 100 ml distilled water, while the specimens annealed at 260 °C were treated using dilute sulfuric acid. Their microstructures were displayed in Fig. 2. Using mean linear intercept method, the average grain sizes were approximately 70 μm for the fine-grained specimens and 1 mm for the coarse-grained specimens.

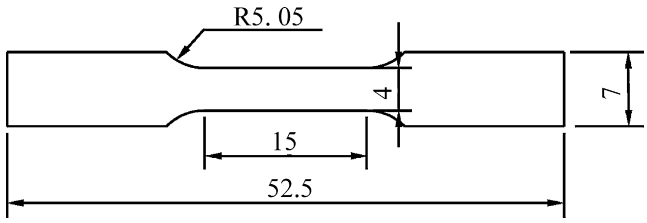

Fig. 1. Specimen configuration (unit: mm).

After mechanical polishing, the bright surface of the specimen was actually covered by re-crystallized films constituted by ultra-fine zinc grains, and beneath the film was a layer of microdeformation twins caused by scratching during mechanical preparation of the specimen [20]. As a result, severe chemical polishing using concentrated nitric acid was employed to get rid of the surface layer. After that, chemical polishing with solution composed of 20 g CrO_3, 1.5 g Na_2SO_4 and 100 ml distilled water was used to make the surface more flat [21]. Then, $50\%H_3PO_4 + 50\%C_2H_5OH$ solution was used to electrically polish the specimen under 13 V dc for 10–15 s to yield clean surface for observation.

Tensile tests were carried out using Instron 8871 fatigue testing machine under strain rates of $10^{-4}\,s^{-1}$, $3 \times 10^{-4}\,s^{-1}$, $10^{-3}\,s^{-1}$ and $10^{-2}\,s^{-1}$ at room temperature in air. After tensile tests, the damage and fracture morphology were observed using optical microscopy and scanning electron microscopy (SEM).

3. Results and discussion

3.1. Deformation and fracture behaviors of specimens with coarse grains

The tensile engineering stress–strain curves for coarse-grained specimens are shown in Fig. 3. It can be seen that both of

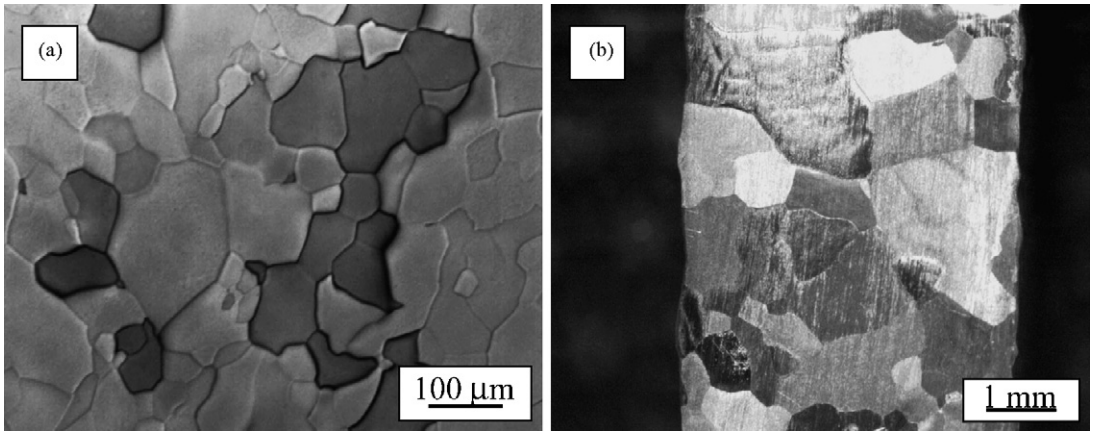

Fig. 2. Microstructures of the specimens: (a) annealed at 150 °C; (b) annealed at 260 °C.

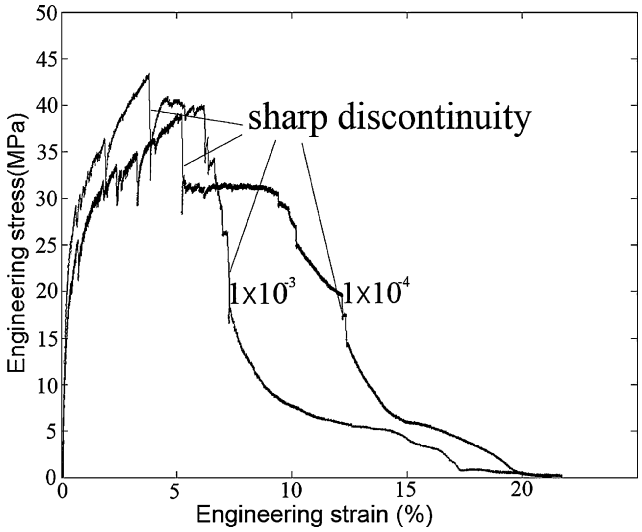

Fig. 3. Tensile engineering stress–strain curves for coarse-grained specimens.

the stress–strain curves display obvious serrated flow behavior after yielding. Actually, stress oscillation took place occasionally during tension, and discontinuities of the tension curves emerged correspondingly. As shown in the figure, the influence of strain rate on serrated flow behavior is not obvious, though higher strain rate lead to more rapid work hardening.

Surface damage observations are shown in Fig. 4. Fig. 4(a) gives a macroscopic view of the cleavage cracks initiating during tension. It was the interlinking of the distributed cleavage cracks that contributed to the final fracture. Fig. 4(b) shows that a cleavage crack initiated beyond grain boundary along slip bands, and its propagation was accompanied by forming of groups of deformation twins (DTs) and kink bands (KBs). Fig. 4(c) and (d) illustrate the grain boundary (GB) penetration process of cleavage cracks in two ways typically, tearing and shearing, respectively.

The fracture surfaces are shown in Fig. 5. Fig. 5(a) is a typical cleavage fractograph. Observation of the details shows typical river markings on the cleavage surface (Fig. 5(b)), with a little tearing and dimples morphology appearing in the vicinity of the grain boundaries (Fig. 5(c)).

Based on the observations above, the sharp discontinuities emerging in the tensile curves were actually related to the intermittent cleavage process. The nucleation of DTs could also induce abrupt stress drop-down during tension for its shearing deformation [22]. However, each twin lamella was normally restricted in a single grain, which made its influence on the

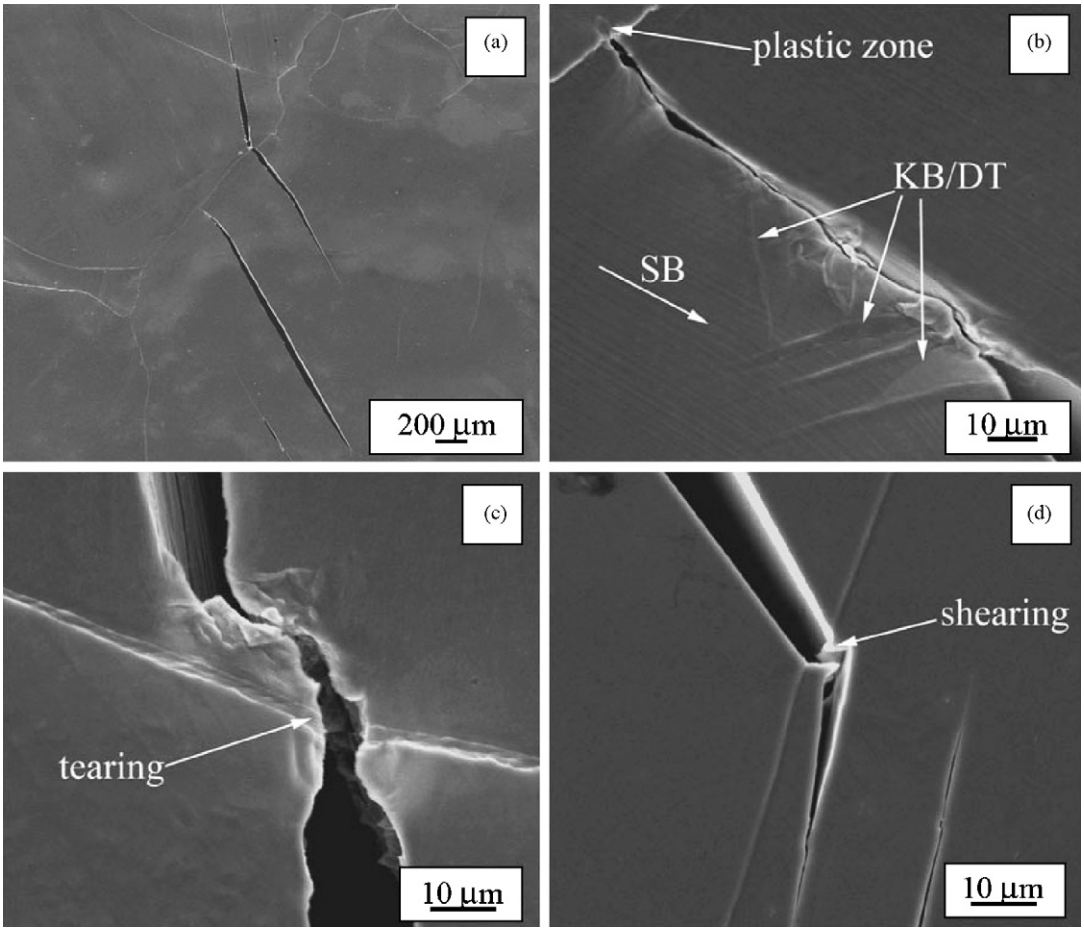

Fig. 4. Cracking of the coarse-grained specimens observed using SEM: (a) damage morphology; (b) cleavage crack initiation beyond grain boundary; (c) crack penetration across GB: tearing; (d) crack penetration across GB: shearing.

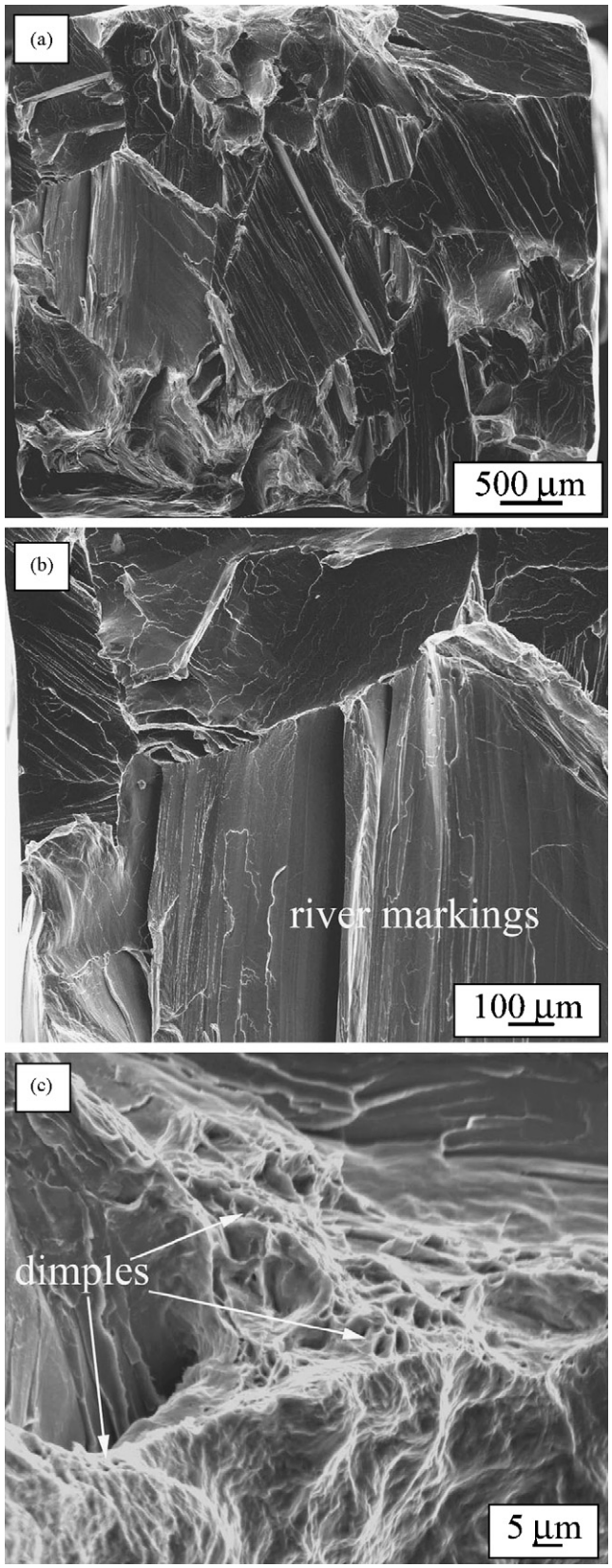

Fig. 5. Brittle fractograph of coarse-grained specimens: (a) macroscopic fracture surface; (b) river markings; (c) dimples and tearing morphology near grain boundary.

mechanical properties of the whole specimen limited. Additionally, the quantity of the DTs of the whole specimen greatly outnumbered the sharp discontinuities in comparison with cleavage cracks.

Gilman [10] investigated the tensile behaviors of bi-crystal zinc and found that the cleavage crack initiated along slip bands instead of beyond or in the upper region of the crack tip. The current observations of the initiation of the cleavage crack beyond GB are consistent with his results. Besides, the observations here showed some details of the propagation process of cleavage crack: in the interior of a grain, crack propagation was accompanied by formation of DTs and KBs along; while in the vicinity of GB, cleavage crack first induced a plastic zone ahead (Fig. 4(b)), and then crossed the GB as the strain accumulating. Burr and Thompson [11,12] had discussed the effects of DTs and KBs accompanying crack propagation and thought that they relaxed the inconsistent strain caused by crack propagation. The two notable different modes for crack to pass through GB in Fig. 4(c) and (d) should be related to the type of the GB. The twist GB penetration required torsion of the material in the vicinity of the GB, while the tilt GB penetration required only simple change of the propagation direction of the cleavage crack. Schmitz et al. [14] used to consider the effects of GB orientation on the process of crack penetrating into neighbor grains in terms of effective surface energy of the crack, and found that for twist GB the process increased the effective surface energy far more than for tilt GB. From the present observations, this might be caused by the severe distortion during cleavage crack penetrating across the twist GB into the neighbor grain.

Generally, the damage and fracture of coarse-grained zinc are primarily controlled by its particular crystal structure. The effects of GB on the damage and fracture of coarse-grained zinc are to block dislocation motion and induce cleavage cracking. The whole process can be simply considered as consolidation of fracture of a cluster of mono- and bi-crystals.

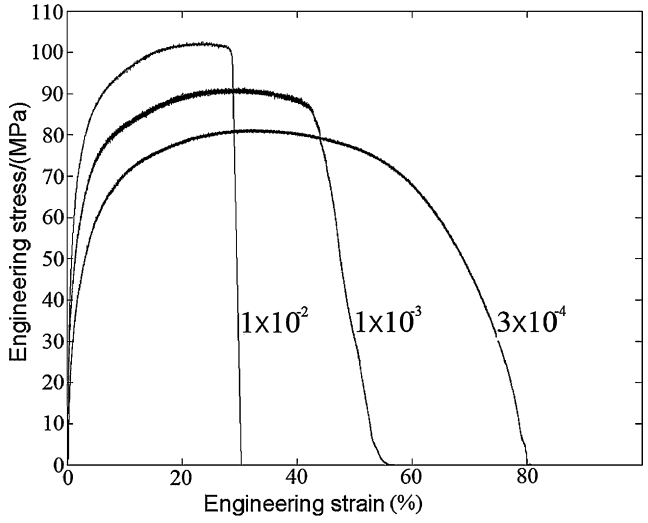

Fig. 6. Tensile engineering stress–strain curves for fine-grained specimens.

3.2. Deformation and fracture behaviors of specimens with fine grains

When the fine-grained specimens were subjected to tension at strain rates of $3 \times 10^{-4}\,s^{-1}$, $10^{-3}\,s^{-1}$ and $10^{-2}\,s^{-1}$, the stress–strain curves displayed apparently different features in comparison with those specimens with coarse grains, as shown in Fig. 6. On one hand, all the tensile stress–strain curves are very smooth before obvious decrease of the tensile stress. On the other hand, the fracture stage which was characterized by continuous decrease of the tensile stress was strongly influenced by strain rate. It was observed that the tensile stress fell gradually at low strain rate ($3 \times 10^{-4}\,s^{-1}$), decreased near linearly at higher strain rate ($1 \times 10^{-3}\,s^{-1}$), and dropped abruptly at the highest strain rate ($1 \times 10^{-2}\,s^{-1}$).

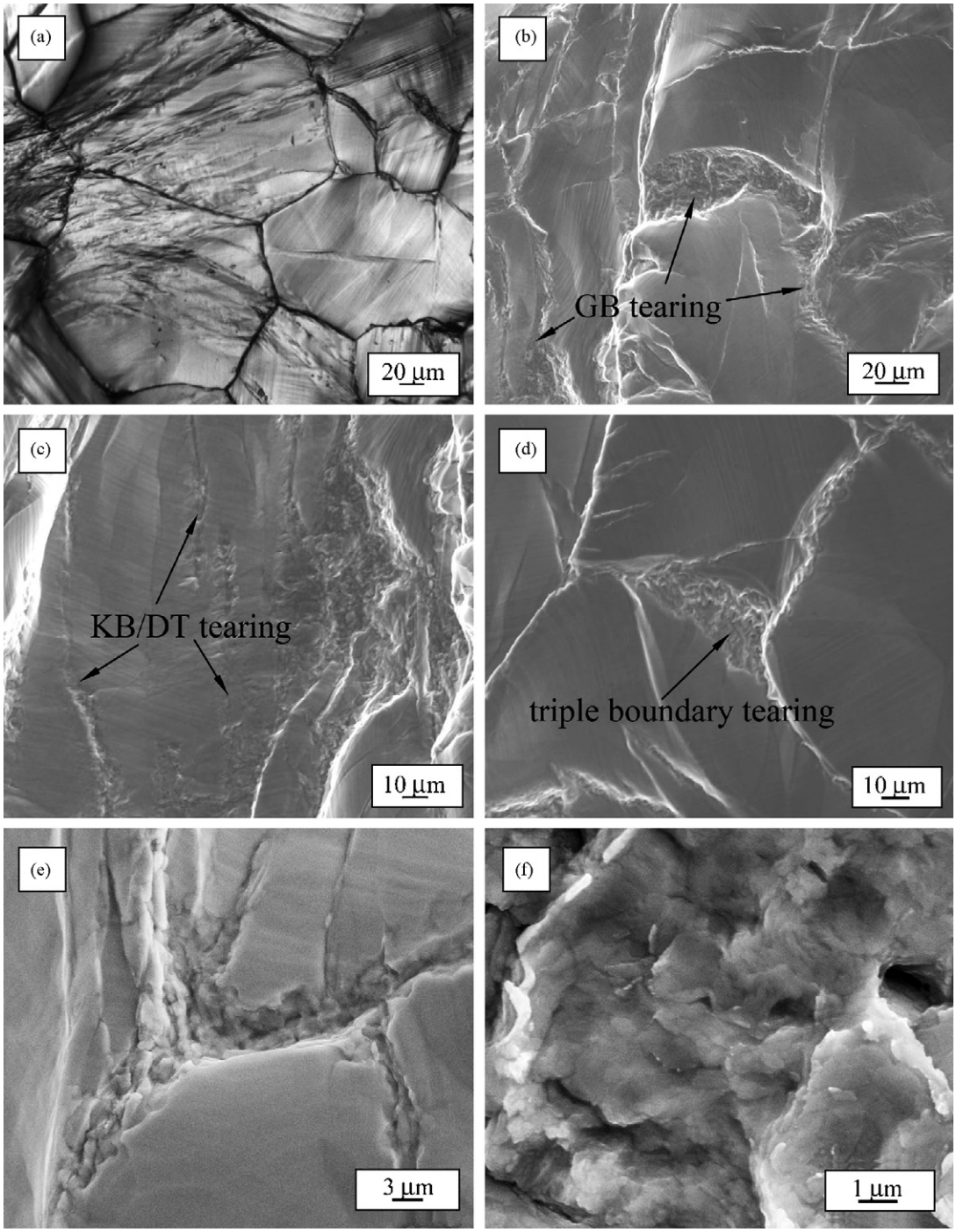

Fig. 7. Surface damage of fine-grained specimen under strain rate of 3×10^{-4}: (a) deformed surface before necking; (b) grain boundary tearing crack; (c) tearing cracks along boundaries of KBs and DTs; (d) tearing crack near triple grain boundary; (e)–(f) damage of grain boundary under high magnification, which shows viscous flow feature.

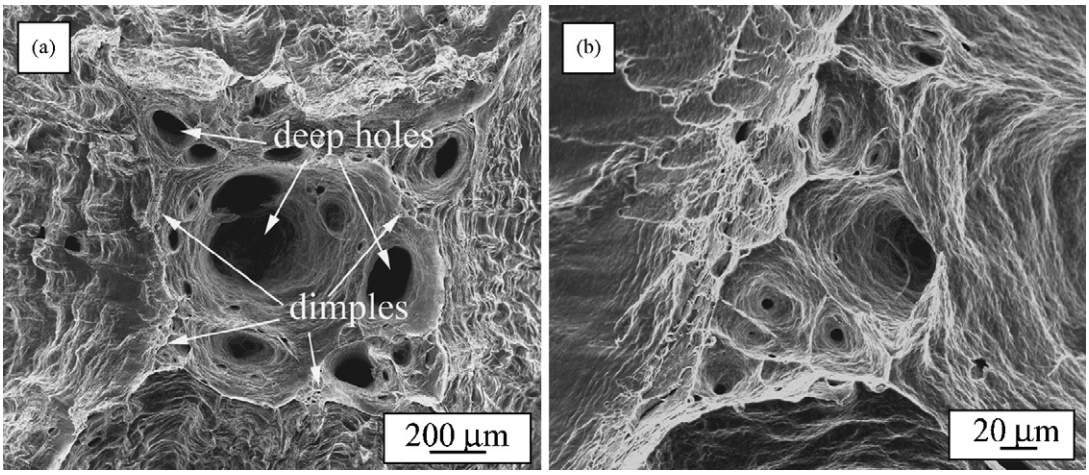

Fig. 8. Fractograph of fine-grained-specimen under strain rate of 3×10^{-4}: (a) deep holes and dimples; (b) high magnification of dimples.

The damage morphology under strain rate of $3 \times 10^{-4}\,s^{-1}$ is shown in Fig. 7. Before necking, deformation bands interlacing with each other formed the deformed surface with no crack initiation, as shown in Fig. 7(a). After necking, surface damage began to develop. From Fig. 7(b)–(d), it was found that tearing cracks could develop along GB, KB, DT as well as triple GB, forming coarse strips. The details of the coarse strips were investigated under high magnification and shown in Fig. 7(e) and (f), which were characterized by viscous flow morphology.

Observations on the fracture surface are shown in Fig. 8. The fracture surface is composed of deep holes and small dimples. Obviously, the size of holes and dimples are rather different.

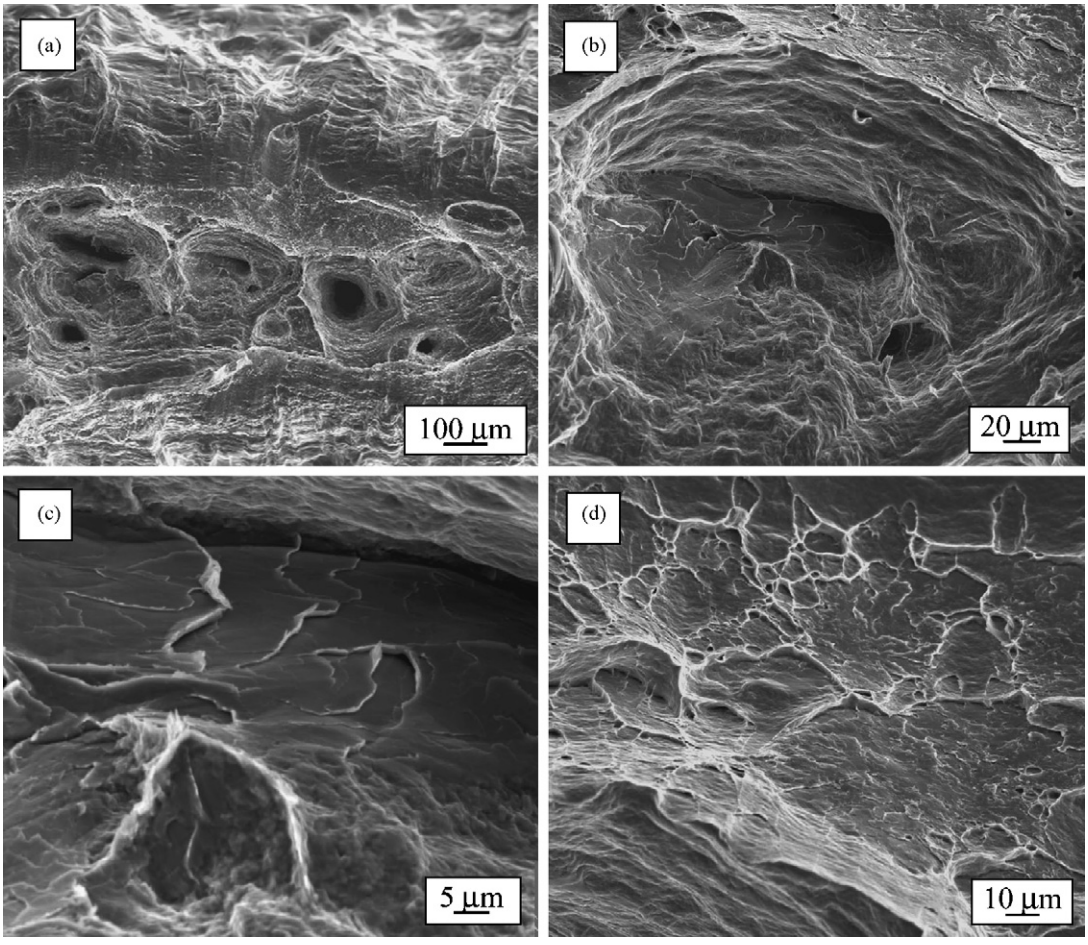

Fig. 9. Fractograph of fine-grained specimen under strain rate of 1×10^{-3}: (a) fractograph; (b) cleavage planes in the center of a dimple; (c) details of (b); (d) interlaced structure of dimples and cleavage facets.

Small dimples mainly distribute along GBs, while large holes situate in the center of specimen.

Under strain rate of $1 \times 10^{-3}\ s^{-1}$, the evolution of the surface damage is similar to that under strain rate of $3 \times 10^{-4}\ s^{-1}$. However, its fracture surface is different, as shown in Fig. 9. Although the fracture surface still consisted of holes and dimples (Fig. 9(a)), cleavage lamellae could be found in the core of large holes (Fig. 9(b and c)). At the same time, composite structure (Fig. 9(d and e)) formed by dimples interlacing with quasi-cleavage morphology is also observed.

Brittle fracture under strain rate of $1 \times 10^{-2}\ s^{-1}$ led to fracture perpendicular to tensile axis. The surface damage shown in Fig. 10(a) indicates that the specimen failed in cleavage mode. However, different from specimens with coarse grains, the cleavage cracks mainly concentrate in the frontier of fracture surface. Its fractograph exhibits typical quasi-cleavage, as shown in Fig. 10(b)–(d).

For specimens with small grain size, the deformation would distribute more homogeneously due to more grains during tension. This made it more versatile to accommodate large plastic deformation without forming intense local stress concentration. As a result, tension of fine-grained specimens always proceeded smoothly instead of showing serrated flow behavior. Additionally, deformation details shown in Fig. 7(a) indicated that the deformation intensity of zinc grains varied with orientation. The grains which oriented easy to deformation sustained most of the plastic strain, and their homogenous distribution effectively prevented the formation of local intense stress concentration and impeded cleavage initiation during the primary stage of tension.

Under strain rate of $3 \times 10^{-4}\ s^{-1}$, it was notable that tearing of grain boundaries, replaced cleavage, becoming the fundamental mechanism of failure for fine-grained specimen. Tearing cracks along TB as well as KB were also observed. These phenomena indicated that at room temperature the binding strength of interfaces in polycrystalline zinc was relatively weak. Thus, along with GB sliding and grain rotation, tearing cracks developed along interfaces gradually. Chang and Grant [23] used to make a detailed analysis of the cracks initiation and propagation along GBs at elevated temperature in aluminum. He considered that boundary sliding could induce intense tensile stress normal to the GB surfaces, leading to crack initiation and subsequent propagation along GB. The surface damage observation was consistent with his conclusion (Fig. 7(b)) and indicated that the normal stress perpendicular to the GB surfaces induced cracking. Moreover, the present observations indicated that cracks could also developed along TBs as well as KB boundaries, and the damage morphology suggested that the normal stress was the underlying cause either (Fig. 7(c)).

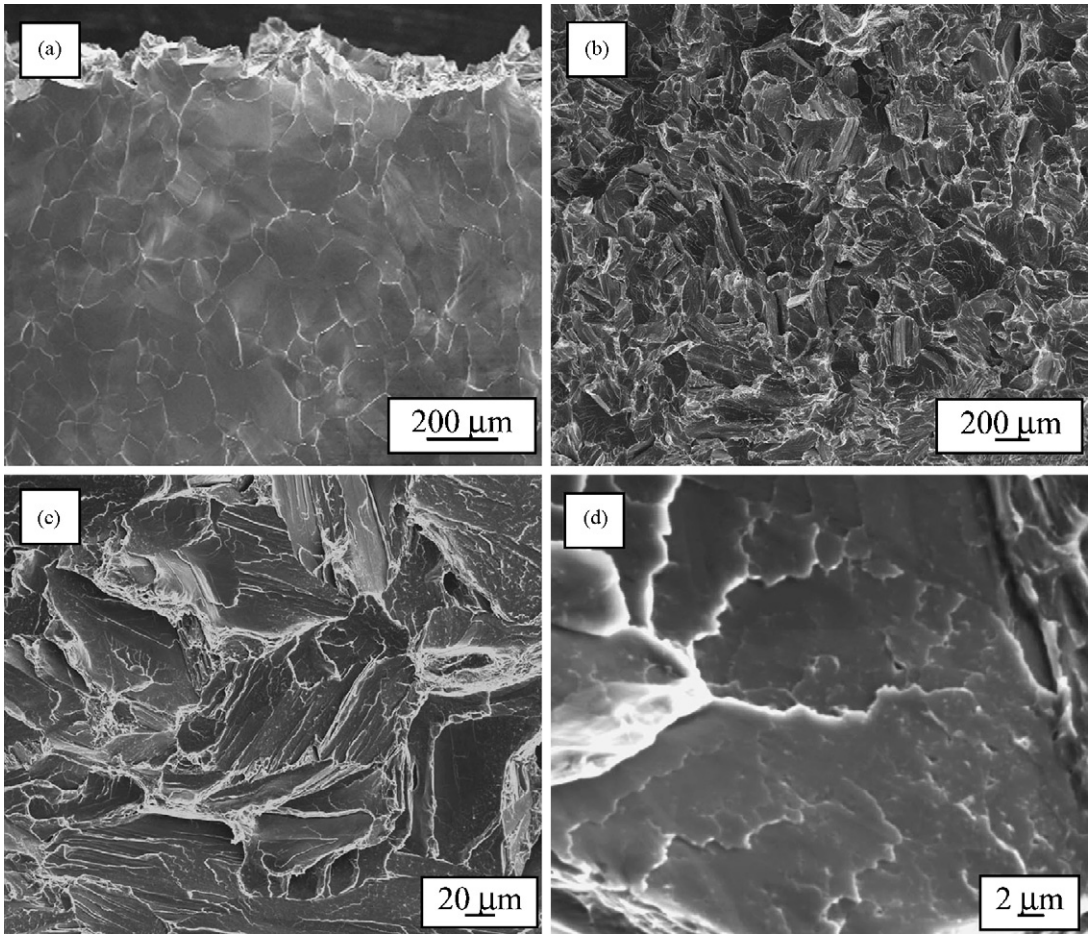

Fig. 10. Surface crack morphology and fractograph of fine-grained specimen at strain rate of 1×10^{-2}: (a) surface damage; (b) macroscope fractograph; (c) high magnification of (b); (d) details of quasi-cleavage.

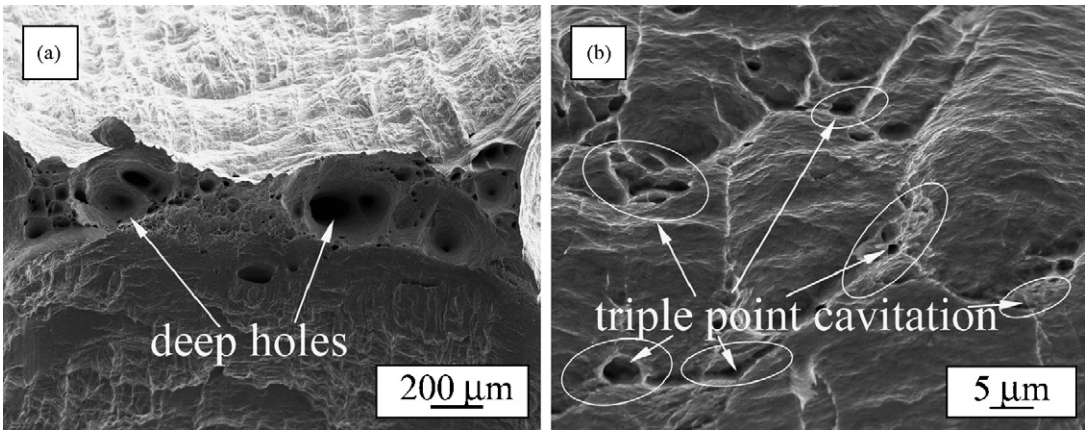

Fig. 11. Fractograph of fine-grained specimen with rectangular cross-section: (a) position of deep holes; (b) cavity nucleation at GB triple-points.

In addition to the surface damage, the fractograph under strain rate of $3 \times 10^{-4}\ s^{-1}$ also showed that the damage and fracture process developed along GBs without cleavage. For deeper investigation of the formation of deep holes and small dimples, tension of a rectangular specimen was carried out at the same strain rate. The fracture surface is shown in Fig. 11. It is observed that the large holes shifted to the sides of the fracture surface (Fig. 11(a)). The differences between rectangular and square specimens lie in that there would be two centers emerging under three-dimensional tensile stress caused by necking instead of only one forming in the center of the square specimen (illustrated in Fig. 12), which corresponds to the shift of the position of the deep holes. Additionally, it is also shown that small dimples mainly formed in GB triple junctions (Fig. 11(b)). The deformation near triple junctions has been investigated by Crossman and Ashby [24], and Gifkins [25], and was in situ observed by Ding et al. [26]. The formation of dimples was considered as the result of accommodation of grain boundary sliding through localized movement of dislocations and directional diffusion of atoms. It was likely that the deep holes evolved from dimples initiated at GB triple junctions, and grew up gradually under the three-dimensional tensile stress caused by necking. The coalescence of those deep holes and dimples led to the final fracture.

The interlacing of cleavage and dimples morphology at strain rate of $1 \times 10^{-3}\ s^{-1}$ indicated that local cleavage developed during fracture. This explained the formation of near linear tension curve, which was not very smooth in Fig. 6. Likewise, the damage cracks which were highly concentrated near the fracture surface instead of distributed along the whole specimen and the quasi-cleavage fractograph are consistent with the abrupt drop-down of stress at strain rate of $1 \times 10^{-2}\ s^{-1}$. Obviously, under high strain rate, the deformation and fracture were controlled by cleavage. This is natural. As cleavage fracture can relatively release deformation energy rapidly, it is favored under high strain rate. In microscopic deformation view, when local stress concentration could not be effectively accommodated by deformation of GBs, the local lattice distortion would aggravate and cleavage would initiate subsequently.

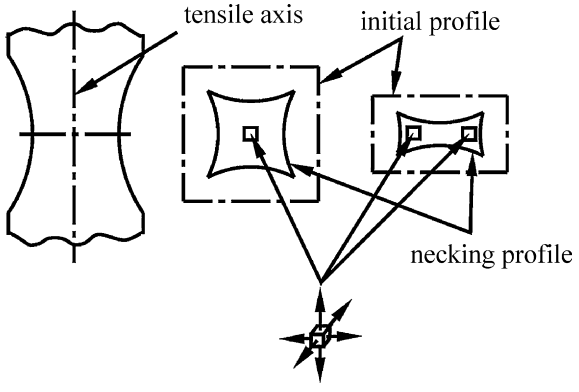

Fig. 12. The position of the three-dimensional tensile stress centers caused by necking.

4. Conclusion

Different from traditional concept that zinc is susceptible to brittle cleavage fracture resulted from its particular crystal structure, the ductile inter-crystalline facture is optional when polycrystalline zinc with fine grains is subjected to low strain rate deformation, and the damage could take place not only along GBs but also along TBs as well as KB boundaries. Based on the observation, the inter-crystalline fracture was controlled by tearing of interfaces microscopically.

The effects of grain size and strain rate on damage and fracture modes of pure zinc were notable. Large grain size and high strain rate led polycrystalline zinc specimen prefer to fail in the form of trans-crystalline cleavage fracture. Whereas small grain size and low strain rate impeded cleavage initiation and led polycrystalline zinc turn to fail from tearing cracks developed along GBs, TBs as well as KB boundaries and coalescing of cavities which nucleated at GB triple junctions, forming ductile inter-crystalline fracture.

Acknowledgements

The authors would like to thank H.S. Liu, W. Gao, F.F. Wu, J.T. Fan, and H.F. Zou for material preparation, mechanical tests and SEM observations. This work was financially supported by the “Hundred of Talents Project” by the Chinese Academy

of Sciences, the National Natural Science Foundation of China (NSFC) under grant No. 50571104, and the National Outstanding Young Scientist Foundation for Z.F. Zhang under grant No. 50625103.

References

[1] E.J. Stofel, Ph.D. Thesis, California Institute of Technology, 1962.
[2] J.W. Christian, S. Mahajan, Prog. Mater. Sci. 39 (1995) 1.
[3] H.S. Rosenbaum, Acta Metall. 9 (1961) 742.
[4] M.H. Yoo, J.K. Lee, Philos. Mag. 63 (1991) 987.
[5] J.N. Florando, M. Rhee, A. Arsenlis, M.M. LeBlanc, D.H. Lassila, Philos. Mag. 86 (2006) 795.
[6] S. Koda, H. Yashinaga, J. Inst. Met. 97 (1969) 125.
[7] G.M. Hughes, G.E. Smith, P.E.J. Flewitt, A.G. Crocker, Key Eng. Mater. 348/349 (2007) 41.
[8] H.J. Frost, M.F. Ashby, Deformation-Mechanism Maps: The Plasticity and Creep of Metals and Ceramics, Pergamon Press, 1982.
[9] R.L. Bell, R.W. Cahn, J. Inst. Met. 86 (1957/1958) 433.
[10] J.J. Gilman, Trans. AIME 212 (1958) 783.
[11] D.J. Burr, N. Thompson, Philos. Mag. 7 (1962) 1773.
[12] D.J. Burr, N. Thompson, Philos. Mag. 12 (1965) 229.
[13] C. Messmer, D. Dew-Hughes, J.C. Bilello, Philos. Mag. 47 (1983) 635.
[14] H.A. Schmitz, D. Dew-hughes, J.C. Bilello, J. Mater. Res. 4 (1989) 1182.
[15] H. Li, Q.Q. Duan, X.W. Li, Z.F. Zhang, Mater. Sci. Eng. A 466 (2007) 38.
[16] H. Naziri, R. Pearce, Acta Metall. 22 (1974) 1321.
[17] P. Málek, Mater. Sci. Eng. A 268 (2006) 132.
[18] R. Parisot, S. Forest, A. Pineau, F. Grillon, X. Demonet, J.-M. Mataigne, Met. Mater. Trans. A 35A (2004) 797.
[19] R. Parisot, S. Forest, A. Pineau, F. Grillon, X. Demonet, J.-M. Mataigne, Met. Mater. Trans. A 35A (2004) 813.
[20] L.E. Samuels, G.R. Wallwork, J. Inst. Met. 86 (1957/1958) 43.
[21] R.C. Brandt, K.H. Adams, T.J.R. Vreeland, J. Appl. Phys. 34 (1963) 587.
[22] T. Richeton, P. Dobron, F. Chmelik, J. Weiss, F. Louchet, Mater. Sci. Eng. A 424 (2006) 190.
[23] H.C. Chang, N.J. Grant, J. Met. Trans. AIME 206 (1956) 544.
[24] F.W. Crossman, M.F. Ashby, Acta Metall. 23 (1975) 425.
[25] R.C. Gifkins, Met. Trans. 7A (1976) 1225.
[26] Y. Ding, C.Q. Wang, M.Y. Li, H.S. Bang, Mater. Lett. 59 (2005) 697.